Metabolic programming a lean phenotype by deregulation of RNA polymerase III

Ian M. Willis[a,b,1], Robyn D. Moir[a], and Nouria Hernandez[c]

[a]Department of Biochemistry, Albert Einstein College of Medicine, Bronx, NY 10461; [b]Department of Systems and Computational Biology, Albert Einstein College of Medicine, Bronx, NY 10461; and [c]Center for Integrative Genomics, Faculty of Biology and Medicine, University of Lausanne, 1015 Lausanne, Switzerland

Edited by Dieter Söll, Yale University, and approved October 15, 2018 (received for review September 10, 2018)

As a master negative regulator of RNA polymerase (Pol) III, Maf1 modulates transcription in response to nutrients and stress to balance the production of highly abundant tRNAs, 5S rRNA, and other small noncoding RNAs with cell growth and maintenance. This regulation of Pol III transcription is important for energetic economy as mice lacking *Maf1* are lean and resist weight gain on normal and high fat diets. The lean phenotype of *Maf1* knockout (KO) mice is attributed in part to metabolic inefficiencies which increase the demand for cellular energy and elevate catabolic processes, including autophagy/lipophagy and lipolysis. A futile RNA cycle involving increased synthesis and turnover of Pol III transcripts has been proposed as an important driver of these changes. Here, using targeted metabolomics, we find changes in the liver of fed and fasted *Maf1* KO mice consistent with the function of mammalian Maf1 as a chronic Pol III repressor. Differences in long-chain acylcarnitine levels suggest that energy demand is higher in the fed state of *Maf1* KO mice versus the fasted state. Quantitative metabolite profiling supports increased activity in the TCA cycle, the pentose phosphate pathway, and the urea cycle and reveals changes in nucleotide levels and the creatine system. Metabolite profiling also confirms key predictions of the futile RNA cycle hypothesis by identifying changes in many metabolites involved in nucleotide synthesis and turnover. Thus, constitutively high levels of Pol III transcription in *Maf1* KO mice reprogram central metabolic pathways and waste metabolic energy through a futile RNA cycle.

RNA polymerase III | Maf1 | metabolic inefficiency | futile cycle | metabolomics

Maf1 is a conserved negative regulator of transcription by RNA polymerase (Pol) III. The protein controls Pol III transcription in response to changing nutritional, environmental, and cellular stress conditions to balance the production of highly abundant tRNAs, 5S rRNA, and other small noncoding RNAs with ribosome biogenesis, cell growth, and maintenance (1–3). In *Saccharomyces cerevisiae*, the signaling network mediating these responses controls the phosphorylation state of Maf1 and thereby regulates its interaction with Pol III, leading to the inhibition of transcription. At the same time, changes in the phosphorylation state of initiation factor and polymerase subunits alter the functions of these complexes to promote Maf1-dependent repression (1). Similar mechanisms are thought to control Pol III transcription in higher eukaryotes. The phosphorylation of human Maf1 by the mechanistic target of rapamycin complex 1 controls its interaction with Pol III (1). However, the relationship between Maf1 phosphoregulation and parallel changes to the mammalian Pol III transcription machinery induced by nutrient deprivation or stress are less well defined (4).

Aside from ensuring appropriate levels of RNA synthesis under a wide range of conditions, tight control of Pol III transcription is considered to be important for energetic economy. Given that tRNA and 5S rRNA make up about one-fifth of total cellular RNA and that rapidly dividing yeast cells duplicate this RNA population every 90 min, the failure of *maf1*Δ cells to down-regulate Pol III transcription as nutrients are depleted (5) is expected to incur an energetic penalty. Although the phenotypic consequences of inappropriate energy expenditure under these conditions are unclear, deficiencies in energy availability may underlie reductions in chronological lifespan (6, 7) and sporulation efficiency (8) reported for haploid and diploid *maf1*Δ strains, respectively. Studies in higher eukaryotes support the concept that Maf1 contributes to metabolic efficiency since mice with a whole body knockout of *Maf1* are lean and resist weight gain on normal and high fat diets (9). Multiple factors contribute to these changes, including a lower daily food intake and a slightly smaller body size. Metabolic changes are also involved since body weight differences persist when food intake is normalized by pair feeding, and energy expenditure, measured by indirect calorimetry, is increased although the mice are not physically more active.

The known metabolic changes in *Maf1* KO mice are consistent with their lean phenotype. Lipolysis is increased in white adipose tissue and autophagy/lipophagy is increased in the liver (9). Accordingly, liver triglycerides are lower despite a modest increase in lipogenesis and the levels of many amino acids and their downstream metabolites (e.g., the polyamine spermidine, a known inducer of autophagy) are increased. Changes in amino acid levels and polyamines are also apparent in skeletal muscle, suggesting that autophagy may be increased in other tissues. Together, the increase in catabolism of lipids and proteins indicates that *Maf1* KO mice have an increased demand for metabolic energy. Experiments to address the source of this demand ruled out elevated uncoupling of the mitochondrial proton gradient in brown and white adipose tissue. Instead, the energy sink

Significance

As a repressor of transcription by RNA polymerase (Pol) III, Maf1 is thought to play an important role in the energetic economy of cells by controlling the synthesis of highly abundant tRNAs and 5S rRNA. Accordingly, *Maf1* knockout mice are lean, resist weight gain on normal and high fat diets, and up-regulate catabolic processes to meet their increased demand for cellular energy. The origin of this energy demand is proposed to reside in a futile cycle of RNA synthesis and turnover that is enhanced by constitutive Pol III transcription. We present metabolomic evidence supporting this mechanism. We find that central metabolic pathways are reprogrammed in the liver of *Maf1* knockout mice to direct substrates toward energy generation and nucleotide synthesis.

Author contributions: I.M.W., R.D.M., and N.H. designed research; I.M.W. and R.D.M. performed research; I.M.W. and R.D.M. analyzed data; and I.M.W. wrote the paper.

The authors declare no conflict of interest.

This article is a PNAS Direct Submission.

[1]To whom correspondence should be addressed. Email: ian.willis@einstein.yu.edu.

This article contains supporting information online at www.pnas.org/lookup/suppl/doi:10.1073/pnas.1815590115/-/DCSupplemental.

Published online November 14, 2018.

was suggested to result primarily from elevated Pol III transcription. Northern blotting of short-lived precursor tRNAs showed that Pol III transcription was increased three- to ninefold in a variety of tissues but the levels of specific mature tRNAs and the size of the tRNA population as a fraction of total RNA was largely unchanged. This led to the idea that futile cycling of highly abundant Pol III transcripts, especially tRNA, is a critical driver of metabolic changes in the mice (9).

Studies of transcription and metabolism conducted to date on *Maf1* KO mice have focused mostly on the fasted state since differences with wild-type (WT) mice were expected to be greater under conditions that cause Maf1-dependent repression. However, recent work indicates that mammalian Maf1, unlike yeast, functions as a chronic repressor (10). In proliferating IMR90htert cells under nutrient-replete conditions, knockdown of Maf1 increases the genome-wide occupancy of the polymerase at active Pol III loci and increases nascent tRNA synthesis (11). Increased Pol III occupancy in the liver of *Maf1* KO versus wild-type mice is also seen throughout the diurnal cycle (12). These data suggest that the metabolic effects of unrestrained Pol III transcription might also be apparent in the fed state. Here, we examine this possibility as we explore the broader effects of the *Maf1* KO on central metabolism, including nucleotide synthesis and breakdown pathways that are at the heart of the futile RNA cycling hypothesis.

Results

Comparison of Metabolite Profiles in Fed and Fasted Wild-Type and *Maf1* KO Liver. To assess the metabolic effect of the *Maf1* KO in the fed state, we conducted targeted metabolite profiling of liver from wild-type and *Maf1* KO mice after an overnight fast and 5 h of refeeding using the same analytical LC-MS/MS platform employed in our previous studies. As was the case for fasted mice (9), principal components analysis (PCA) readily distinguished the metabolite profiles of fed wild-type and *Maf1* KO mice (*SI Appendix*, Fig. S1*A*). We then compared the effect of the *Maf1* KO on the relative abundance of metabolites (KO/WT) in the fasted and fed state. A larger number of amino acids were significantly elevated in *Maf1* KO versus wild-type liver in the fed state compared with the fasted state (13 vs. 7 amino acids, $P < 0.05$, Fig. 1 and Dataset S1). Moreover, the average fold change in amino acid level in *Maf1* KO tissue was also higher in the fed state (2.0 ± 0.03 vs. 1.66 ± 0.07, SEM, for amino acids with $P < 0.05$ in Dataset S1). The greater magnitude and number of amino acids that were altered in fed *Maf1* KO mice suggests increased protein catabolism to support a relatively greater energetic demand in this condition compared with the fasted state. Other notable changes common to both fed and fasted conditions include increased levels of the polyamine spermidine, consistent with the induction of autophagy in the knockout (9), and increased levels of carnitine and several short and medium chain acylcarnitine species (e.g., C3, C5-OH (C3-DC-M), C7-DC) (Fig. 1 and Dataset S1). These changes are indicative of elevated levels of oxidation of amino acids and/or fatty acids in the knockout (13). Strikingly, in the fed state but not the fasted state, the levels of many long-chain acylcarnitines (C12–C18) were substantially reduced (two- to sevenfold), indicating an increase in the relative level of fatty acid oxidation in *Maf1* KO liver under feeding conditions. This difference was not due to the failure of overnight fasted *Maf1* KO mice to feed during the 5-h period before tissue harvest; both wild-type and *Maf1* KO mice had distended stomachs due to food intake. Thus, the apparent increase in fatty acid oxidation in the fed state reflects an ongoing energy demand in *Maf1* KO animals that is not fully met by the ingested food.

Loss of Maf1 Impacts Central Metabolic Pathways. Given the more pronounced effects of the *Maf1* KO on amino acid and acylcarnitine levels in the fed state (Fig. 1), we chose to further explore changes in liver metabolism under this condition. We performed a targeted quantitative analysis using capillary electrophoresis-mass spectrometry (CE-MS) focusing on metabolites in central metabolic pathways, reasoning that these pathways would be affected by a transcription-driven increase in demand for metabolic energy. Of the 97 metabolites for which independent measurements were obtained for three wild-type and three *Maf1* KO liver samples, 43 metabolites showed statistically significant differences ($P < 0.05$, Dataset S2), indicative of changes in metabolic flux through the affected pathways. With so many differences, principal components analysis readily distinguished wild-type from *Maf1* KO samples (*SI Appendix*, Fig. S1*B*). Examination of the CE-MS data revealed similar increases in the amounts and types of amino acids compared with LC-MS/MS on the same samples (*SI Appendix*, Table S1). Thus, the high reproducibility of analyses conducted on independently prepared tissue extracts using different platforms validates the observed changes and supports the numerous other differences measured for metabolites that were uniquely profiled by either CE-MS or LC-MS/MS (Datasets S1 and S2).

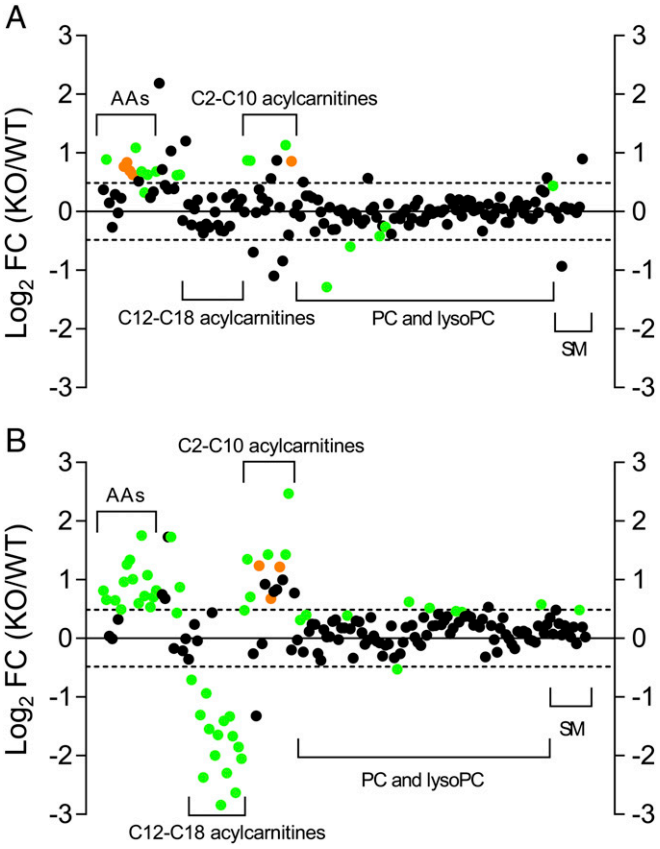

Fig. 1. Biocrates metabolite profiling of wild-type and *Maf1* KO liver from fed and fasted mice. Log_2 fold change (KO/WT) is plotted for samples from overnight fasted mice ($n = 5$ per group) (*A*) and for overnight fasted and 5-h refed mice ($n = 3$ per group) (*B*). Data for 164 metabolites are plotted in the same order from *Left* to *Right* as in Dataset S1. Data for two metabolites in *B*, ornithine and α-amino adipate, are outside the axis limits. Amino acids (AAs), long-chain acylcarnitines (C12–C18), short and medium chain acylcarnitines (C2–C10), phosphatidylcholine (PC), lysophosphatidylcholine (lysoPC), and sphingolipids (SM). Dotted lines represent changes of ±1.4-fold. Green and orange data points represent $P < 0.05$ and $P < 0.1$, respectively. A subset of the data in *A* was reported previously in ref. 9. The complete dataset is plotted here in accordance with a Creative Commons license (CC-BY).

Most glycolytic and TCA cycle intermediates were not significantly affected. However, pyruvate and acetyl CoA levels were markedly lower and there was a trend toward higher levels of acetoacetyl CoA in the knockout (Dataset S2). These three metabolites are linked by successive reactions at the interface of glycolysis, the TCA cycle, and the catabolism of ketogenic and aromatic amino acids suggesting increased flux through one or more of these pathways (Fig. 2*A*). Enhanced TCA cycling in the *Maf1* KO is consistent with the higher energetic demands resulting from metabolic inefficiency and is supported by the increased oxygen consumption of liver homogenates (9) and by lower levels of acetyl CoA and higher levels of spermidine (Datasets S1 and S2). These metabolites are known to regulate the irreversible oxidative decarboxylation of pyruvate to acetyl CoA catalyzed by pyruvate dehydrogenase via effects on the activities of pyruvate dehydrogenase kinases and phosphatases (14). Accordingly, Western blotting of the pyruvate dehydrogenase E1α subunit (PDHA1) with a phospho-specific antibody to regulatory site 1 (Ser293) showed generally lower levels of phosphorylation in liver extracts from fed *Maf1* KO versus wild-type mice (Fig. 2*B*). By comparison, the total amount of E1α subunit was not substantially changed. Thus, the phosphorylated (i.e., inhibited) fraction of the enzyme was determined to be lower in the knockout (0.69 ± 0.09, $P = 0.02$). These data are consistent with the view that pyruvate dehydrogenase activity and consequently, TCA cycle flux, is increased in the liver of *Maf1* KO mice.

Metabolites of the urea cycle and the purine nucleotide cycle (PNC), both of which interconnect to the TCA cycle, were also affected in the liver of fed *Maf1* KO mice (Fig. 2*A*). The TCA and urea cycles are coupled by the aspartate-argininosuccinate shunt (15) which enables fumarate produced in the cytoplasm as a byproduct of the urea cycle to be returned to the mitochondria and the TCA cycle as malate (Fig. 2*A*). Increased urea cycle flux, presumably to remove excess ammonia generated by amino acid deamination and nucleotide breakdown in the knockout (see below), is strongly indicated by the elevated levels of argininosuccinate, urea, ornithine, citruilline, and *N*-acetylglutamate, an obligate allosteric activator of carbamoyl phosphate synthase I (CPS1) which catalyzes the rate-limiting first step in the pathway (16, 17) (Fig. 2*A*). In addition, the citrulline–ornithine ratio, an indicator of urea cycle flux, was significantly lower in the knockout, consistent with increased hydrolysis of arginine into ornithine and urea (i.e., increased flux) (Dataset S2). The PNC operates in the cytoplasm where it promotes energy metabolism and TCA cycle anaplerosis (18, 19). In exercising muscle, the PNC, like the urea cycle, converts aspartate to fumarate which can be returned to the TCA cycle to increase oxidative phosphorylation (20). In *Maf1* KO liver, PNC perturbations are indicated by reduced levels of IMP and increased adenylosuccinate (Fig. 2*A*). Both the urea cycle and the PNC are energy consuming: Three ATPs and one pyrophosphate are hydrolyzed with each turn of the urea cycle while one GTP is hydrolyzed in the PNC. Thus, increased flux through these cycles contributes to the overall energy expenditure of *Maf1* KO mice.

Nucleotide Synthesis. A central pillar of the hypothesis that wasteful metabolism drives energy expenditure in *Maf1* KO mice is the notion that unrestrained transcription by Pol III must be sustained by elevated levels of nucleotide synthesis. Nucleotide synthesis is energetically costly, requiring 7–10 ATP equivalents per NTP (depending on the base) for de novo synthetic pathways (21). The precursors for nucleotide synthesis are provided by several feeder pathways including glycolysis and the pentose phosphate pathway (PPP). These pathways funnel glucose and glycolytic intermediates through oxidative and nonoxidative branches of the PPP leading to ribose-5-phosphate, which is subsequently activated to phosphoribosyl diphosphate (PRPP), a critical rate-limiting substrate for nucleotide synthesis in both de novo and salvage pathways (21, 22). Although the levels of numerous intermediates in the nonoxidative PPP were elevated (1.2- to 1.6-fold) in *Maf1* KO liver, suggesting a trend, individual metabolites did not reach statistical significance (Dataset S2). In contrast, the 1.7-fold increase in PRPP was significant ($P = 0.0027$) and supports the view that flux through nucleotide synthesis pathways is increased in *Maf1* KO mice (Fig. 3). Elevated flux through the oxidative branch of the PPP is suggested by the decrease in the level of $NADP^+$ (Dataset S2), two molecules of which are consumed in this pathway (21). Additional evidence consistent with elevated nucleotide synthesis is presented below.

The atomic constituents of purine and pyrimidine rings are derived from glutamine and aspartic acid. In addition, glycine

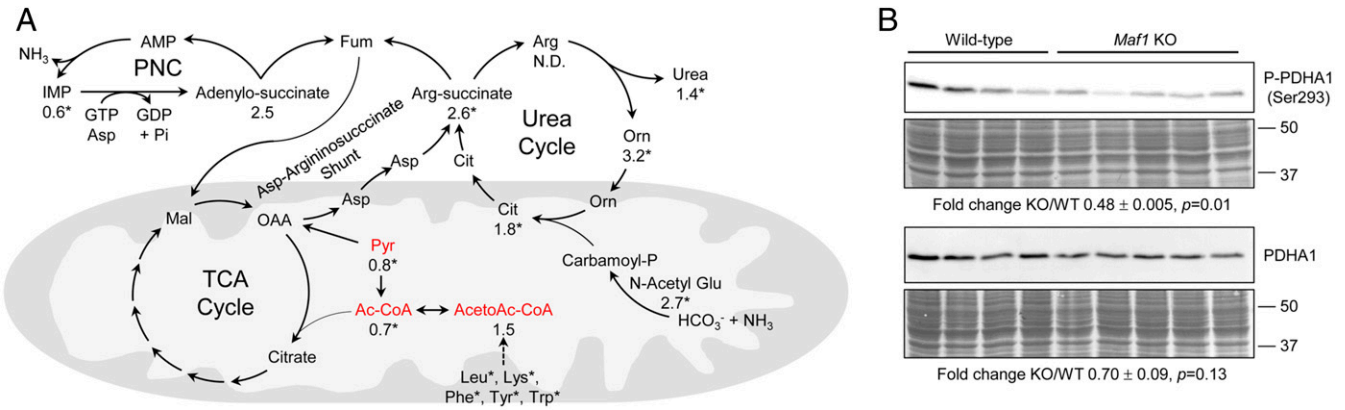

Fig. 2. Central metabolic pathways are impacted in fed liver from *Maf1* KO mice. (*A*) Fold changes (KO/WT) are shown for selected metabolites from Dataset S2 that participate in interconnected pathways, including glycolysis, the TCA cycle, the urea cycle, and the purine nucleotide cycle (PNC). Metabolites in red are at the interface of glycolysis, the TCA cycle, and the catabolism of ketogenic and aromatic acids. Metabolites with statistically significant fold changes ($P < 0.05$, Datasets S1 and S2) are indicated with an asterisk. Numbers without an asterisk indicate a trend ($P < 0.1$) among independent triplicate samples in each group. Metabolites are labeled as in Dataset S2. Arrows indicate chemical transformations or transport of molecules between the mitochondria and the cytoplasm. N.D., not determined. (*B*) Representative Western blots of phospho (Ser293) and total PDHA1 in wild-type ($n = 4$) and *Maf1* KO ($n = 5$) liver extracts (fed state). The corresponding regions of the amido black-stained membranes used for normalization of the PDHA1 signals are shown along with the positions of molecular weight markers (kilodaltons). The fold change (KO/WT) for phospho-PDHA1 from triplicate blots and for total PDHA1 from duplicate blots is indicated under the gels with *P* values determined by a one-sample two-tailed *t* test (38). The ratio of these values shows that the fraction of PDHA1 that is phosphorylated in the *Maf1* KO is reduced.

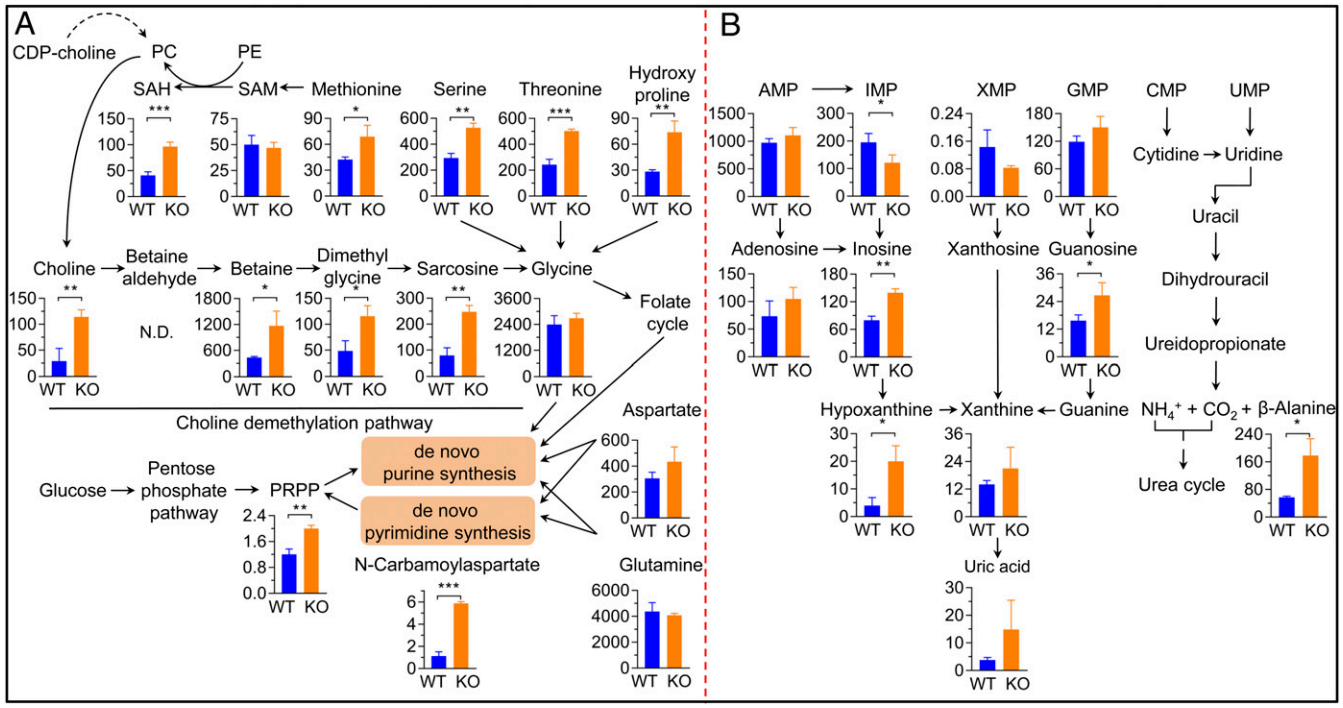

Fig. 3. Absolute levels of metabolites associated with nucleotide synthesis and turnover. (*A*) Metabolites in nucleotide synthesis and feeder pathways. (*B*) Metabolites of nucleotide turnover. Bar graphs show metabolite concentrations (nanomoles/grams of liver ± SD) for independent triplicate liver samples from fed wild-type and *Maf1* KO mice (Dataset S2). Arrows between metabolites represent direct enzyme-catalyzed chemical transformations. The different orientations of arrows emanating from PRPP reflect that purine synthesis occurs on activated PRPP while pyrimidine synthesis to orotate occurs before attachment to PRPP. $*P < 0.05$, $**P < 0.01$, $***P < 0.001$.

contributes to purine ring synthesis both directly and indirectly via folate pathway production of formyl tetrahydrofolate (21). Glutamine, aspartic acid, and glycine are distinct among the majority of amino acids quantified by both the CE-MS and LC-MS/MS platforms in that their levels were not significantly different between wild-type and *Maf1* KO samples (*SI Appendix*, Table S1). This implies that the consumption of these amino acids by downstream processes, such as de novo nucleotide synthesis, is elevated in the knockout. In keeping with this idea, a high demand for glycine in the knockout is indicated by the elevated levels of substrates in all four pathways leading to glycine, namely from serine, threonine, hydroxyproline, and choline (Fig. 3). Notably, every measured metabolite upstream of glycine in the choline demethylation pathway was substantially increased (Fig. 3). Choline is an essential dietary nutrient. It cannot be synthesized by anabolic pathways in the body and thus must be obtained from the diet (23). In previous work we found that *Maf1* KO mice consume slightly less food per day compared with wild-type mice (9). Thus, the fourfold higher level of choline in *Maf1* KO liver cannot be explained by differences in food intake. We deduce that the increase in choline is likely the result of phosphatidylcholine (PC) catabolism (24). Furthermore, with much of the increase in choline apparently being directed toward glycine (Fig. 3), the synthesis of PC may depend more on the phosphatidylethanolamine (PE) methylation pathway than on the CDP-choline branch of the Kennedy pathway. Consistent with this, we observed a significant increase in S-adenosyl homocysteine (SAH), the demethylated product of S-adenosylmethionine (SAM) which serves as the methyl donor in the PE methylation pathway (Fig. 3) and a 2.5-fold reduction in the SAM/SAH ratio ($P = 0.044$, Dataset S2). Finally, the rate of de novo pyrimidine synthesis is limited at two steps; the first step, catalyzed by carbamoyl phosphate synthase II and the fourth step, catalyzed by dihydroorotate dehydrogenase (21). In between these steps, the metabolite *N*-carbamoylaspartate was increased 5.2-fold in the knockout, indicating increased flux through this pathway (Fig. 3). Thus, changes in multiple metabolites indicate that de novo nucleotide synthesis is elevated in the liver of *Maf1* KO mice.

Nucleotide Turnover. While unrestrained transcription by Pol III in the *Maf1* KO leads to an increase in the demand for nucleotides, the RNA products, most of which are tRNAs, do not accumulate above normal levels (9). This suggested the existence of a tRNA homeostatic mechanism to limit the size of the tRNA pool and led to the concept of tRNA futile cycling as a mechanism of energy expenditure. Thus, in the *Maf1* KO, increased tRNA synthesis is expected to be offset by increased turnover of nascent tRNA molecules to maintain the size of the total tRNA pool (9). Experimental support for increased RNA turnover is provided by changes in the levels of metabolites in nucleotide catabolic pathways. For purine catabolism, the concentrations of IMP, inosine, hypoxanthine, and guanosine were all significantly different in knockout versus wild-type liver and the final breakdown product, uric acid, showed substantially higher levels in all *Maf1* KO versus wild-type samples (average KO/WT 3.9 ± 0.74), albeit with a higher variance in the knockout (Fig. 3 and Dataset S2). Pyrimidine catabolism from UMP and CMP generates the corresponding nucleosides as for purines. Cytosine is deaminated to uridine and after hydrolysis of the glycosyl bond, uracil is reduced and further hydrolyzed to yield ammonia and CO_2, which enter the urea cycle, and β-alanine which is excreted in the urine. Notably, β-alanine levels were substantially increased in *Maf1* KO liver (Fig. 3 and Dataset S2). These data support increased rates of nucleotide turnover.

Adenosine Nucleotide Levels and the Phosphocreatine System. The increase in the demand for metabolic energy in *Maf1* KO mice affects the levels of adenosine nucleotides; the amount of ATP,

ADP, and total adenylate was reduced in the liver of these mice (Fig. 4*A*). The same trend was seen for GTP, GDP, and total guanylate (Dataset S2). In addition, the levels of creatine system metabolites, namely creatine, phosphocreatine (PCr) and the nonenzymatic cyclization product, creatinine, were elevated (Fig. 4*B*). The creatine system, which includes the readily reversible activity of mitochondrial and cytoplasmic creatine kinase isoforms, plays an important role in tissues with high, fluctuating energy demands. As a high-energy intermediate, phosphocreatine buffers the hydrolysis of ATP in skeletal muscle and can function as a diffusible energy source from its site of synthesis in the mitochondrial matrix to other sites in the cell where ATP can be regenerated and utilized (25). More recently, the creatine system has been found to play a role in thermogenesis in adipose tissue through a proposed futile substrate cycle in which phosphatase-mediated hydrolysis of PCr promotes continued ATP synthesis (26, 27). In contrast to many other tissues, liver contains very low levels of creatine kinase activity so it is unlikely that futile cycling of phosphocreatine would make a significant contribution to energy expenditure in this tissue. However, the liver is an important site for the synthesis of creatine which is then exported to other tissues (25). Thus, it is possible that enhanced synthesis of creatine in the liver of *Maf1* KO mice may contribute to energy expenditure in other cells and tissues through the mechanisms described above.

Conclusions

The lean phenotype of *Maf1* KO mice is due, in part, to a decrease in metabolic efficiency (9). As a consequence, the catabolism of proteins and lipids is increased through autophagy/lipophagy and lipolysis to generate substrates for energy metabolism (Fig. 4*C*). Based on previous experiments conducted in fasted mice, a futile RNA cycle involving the sustained synthesis and turnover of highly abundant Pol III transcripts, most notably tRNAs, was proposed as the main driver of the increased energy demand of *Maf1* KO animals (9). This hypothesis is strengthened by the finding that Maf1 functions chronically to limit Pol III activity in both proliferating mammalian cells and throughout the diurnal cycle in differentiated mouse tissue (i.e., liver) (11, 12). Changes in liver metabolites under fed and fasted conditions further support this view. Together with the knowledge that precursor tRNA levels are increased in all tested tissues from *Maf1* KO mice (9), the data suggest that Pol III transcription is constitutively elevated in all nucleated cells of these mice.

The increased energy requirements of *Maf1* KO mice appear to be greater in the fed state than in the fasted state. This was initially indicated by indirect calorimetry (9). In the current work, metabolic evidence supporting a relatively higher energy demand in the fed state of *Maf1* KO mice is provided by the reduction in long-chain acylcarnitines, indicative of increased β-oxidation (Fig. 4*C*). This differential in long-chain acylcarnitines was only seen in the fed state (Fig. 1). In contrast, the levels of many amino acids were elevated in the liver of both fed and fasted *Maf1* KO mice although the results again support more pronounced effects on amino acid levels in the fed state (Fig. 1 and Dataset S1). In accordance with the higher energy demand in the knockout, the fate of many of these amino acids involves deamination, requiring increased urea cycle activity (Fig. 2) and allowing entry of the carbon skeletons into the TCA cycle for further oxidation by the electron transport chain (28).

A key prediction of the futile RNA cycling hypothesis is that the synthesis of ribonucleotides must be increased to meet the higher levels of Pol III transcription. Metabolite profiling provided strong support for this view under the guiding principle that altered metabolite levels reflect changes in the rates of the connected consuming or producing reactions (29, 30). Multiple metabolites involved in nucleotide synthesis were affected, including rate-limiting molecules (PRPP) and intermediates in de novo pyrimidine synthesis and the feeder pathways that supply substrates for building purine and pyrimidine rings (Fig. 3). Futile RNA cycling also predicts changes in metabolites involved in the turnover of nucleoside monophosphates generated by RNA degradation. Metabolite profiling confirmed this prediction as well. Consistent with the view that substrate concentration plays a predominant role in determining reaction rates relative to enzyme abundance (31), the metabolic changes evident in our profiling studies appear to have arisen without significant effects on the expression of nucleotide synthesis, nucleotide turnover, or other enzymes of central metabolism (e.g., glycolysis, TCA cycle, electron transport chain, pentose phosphate pathway, urea cycle): Transcriptome and ribosome profiling of liver in the fed state does not reveal changes in the expression of enzymes in these pathways. In support of this, the level of PDHA1, a catalytic and regulatory subunit of pyruvate dehydrogenase which links glycolysis with the TCA cycle and the levels of rate-limiting enzymes in the urea cycle and pyrimidine synthesis were unchanged (Fig. 2*B* and *SI Appendix*, Fig. S2). Instead, Western analysis of phospho-PDHA1 pointed toward a metabolite-based increase in pyruvate dehydrogenase activity. Similar metabolite-based increases in purine and pyrimidine synthesis are expected, given the changes in nucleotide levels (Fig. 4*A*) and other key molecules (PRPP) and the well-known regulation of enzymes in these pathways by allostery and feedback inhibition (21). Accordingly, it appears that by knocking out *Maf1* in the mouse, futile RNA cycling causes a cascade of metabolic changes, effectively reprogramming metabolism to meet the increase in energy demand while directing substrates toward nucleotide synthesis.

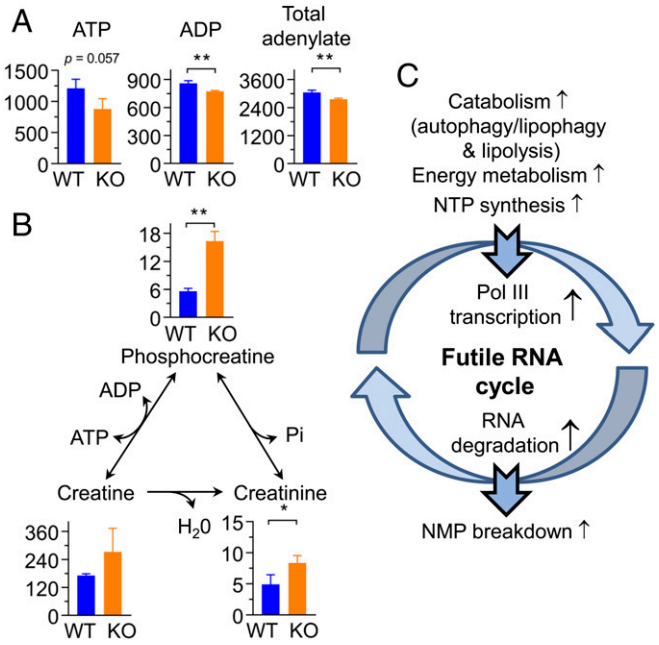

Fig. 4. Energy metabolites are altered in the liver of fed *Maf1* KO mice. (*A*) Levels of ATP, ADP, and total adenylated nucleotides (ATP + ADP + AMP). (*B*) Levels of creatine, phosphocreatine, and the nonenzymatic cyclization product creatinine. Data plotted in *A* and *B* report nanomoles of metabolite/grams of liver ± SD (Dataset S2). (*C*) Scheme illustrating how futile RNA cycling serves as a mechanism of energy expenditure. NMP, nucleoside monophosphate. $*P < 0.05$, $**P < 0.01$.

Materials and Methods

Mice. Studies were performed with wild-type and *Maf1* KO mice on a C57BL/6J background under a protocol approved by the Institutional Animal Care and Use Committee of the Albert Einstein College of Medicine. Mice were

housed at 22 °C on a 12 h light/dark cycle and were fed ad libitum on a breeder chow diet (PicoLab Rodent Diet 20, no. 5058, 21.6% calories from fat) unless otherwise noted.

Metabolite Profiling. Male mice at 24 wk of age were killed after an overnight fast or after an overnight fast and 5 h of refeeding. The liver was rapidly removed, the gall bladder was dissected away, and the tissue was freeze clamped in liquid nitrogen. Tissue was stored at −80 °C. Quantitative or semiquantitative measurements of up to 188 metabolites representing amino acids, biologic amines, acylcarnitines, lysophosphatidylcholines, phosphatidylcholines, and sphingolipids were obtained using an AbsoluteIDQ p180 kit (Biocrates Life Sciences) (32, 33). These studies were performed in the Stable Isotope and Metabolomics Core Facility of the Einstein-Mt Sinai Diabetes Research Center on an ACUITY UPLC-Xevo Tandem Quadrupole (TQ) mass spectrometer (Waters) as recommended (32). For this analysis, tissue samples were ground to powder in a mortar and pestle on dry ice and the frozen powdered tissue (50–100 mg) was weighed into 2-mL screw cap tubes and prechilled on dry ice. Metabolites were extracted by homogenization in methanol containing 5 mM ammonium acetate (8 μL/mg tissue) and processed following the manufacturer's instructions (see also ref. 33). Peak areas were quantified and compared with kit-provided stable isotope-labeled internal standards. Amino acids and biologic amines were quantified from calibration curves. Other metabolites were quantified relative to a single concentration of stable isotope-labeled standard. Six replicates of a pooled tissue extract containing aliquots of all of the samples were used to determine the coefficient of variation for quality control. Absolute quantitative analysis of 116 metabolites in central metabolism was performed by capillary electrophoresis-mass spectrometry using the C-SCOPE platform (Human Metabolome Technologies, Inc.) (HMT) (34, 35). Frozen tissue samples were weighed and homogenized in 50% vol/vol acetonitrile in water containing internal standards. Metabolite peak information, including migration time, *m/z*, and peak area, was obtained and used to assign peaks and to quantify concentrations by reference to internal standards and three-point calibration curves. For both platforms, the concentration of each metabolite in the tissue extracts was calculated in micromoles and then normalized by tissue weight to yield nanomole metabolite per gram of tissue. Unsupervised PCA and exploration of pathways used MetaboAnalyst 4.0 (36) together with analyses provided by HMT.

Western Blotting. Liver extracts from fed mice were prepared by homogenization in RIPA buffer with phosphatase inhibitors (20 mM sodium pyrophosphate, 10 mM glycerol-2-phosphate, 25 mM NaF, and 2 mM sodium orthovanadate) and a cOmplete Mini protease inhibitor mixture (Roche) plus 1 mM PMSF). Extracts (40 μg, determined by Pierce BCA assay) were separated by SDS/PAGE, transferred to nitrocellulose, and protein and immunoblot signals detected with a CCD imager (LAS4000; GE Healthcare). Antibodies were used at a 1:1,000 dilution unless otherwise stated in either 5% BSA or dry milk in 1× TBST as per manufacturer's recommendations. Antibodies were from Santa Cruz Biotechology, Inc [PDH-E1α (D-6):sc-377092; CPS1 (B-1):sc-376190 at a 1:5,000 dilution; vinculin (7F9):sc-73614 at a 1:2,000 dilution; anti-mouse light chain-HRP m-IgGk BP-HRP:sc-516102 at a 1:2,000 dilution], EMD Millipore [anti–phospho-PDHE1-A type1 (Ser293) ABS204], Cell Signaling Technology, Inc (CAD antibody no. 11933), and GE Healthcare (donkey anti-rabbit IgG-HRP NA934V at a 1:5,000 dilution). Total protein, detected by amido black staining, was used as a loading and transfer control after immunodetection (37). Immunoblot and total protein signals were quantified by line peak integration using Image Quant software and were confirmed to be unsaturated and within the linear range as determined by standard curves. Immunoblot signals were normalized to total protein for each lane, the fold change (KO/WT) of each KO sample was determined relative to the mean of the wild-type samples, and an average KO/WT ratio was calculated. The KO/WT ratio from duplicate or triplicate blots was then averaged (38).

Statistics. Data were analyzed for statistical significance using a two-tailed Student's *t* test assuming equal variance between the groups, and the results are expressed as the mean ± SD unless otherwise stated.

ACKNOWLEDGMENTS. We thank Dr. Irwin Kurland for stimulating discussions. This work was supported by National Institutes of Health Grants R01 GM120358 (to I.M.W.), P30 DK020541 (to Einstein–Mt Sinai Diabetes Research Center), and P30 CA013330 (to Albert Einstein Cancer Center), as well as by the University of Lausanne and Swiss National Science Foundation Grant 31003A_169233 (to N.H.).

1. Willis IM, Moir RD (2018) Signaling to and from the RNA polymerase III transcription and processing machinery. *Annu Rev Biochem* 87:75–100.
2. Moir RD, Willis IM (2013) Regulation of pol III transcription by nutrient and stress signaling pathways. *Biochim Biophys Acta* 1829:361–375.
3. Boguta M (2013) Maf1, a general negative regulator of RNA polymerase III in yeast. *Biochim Biophys Acta* 1829:376–384.
4. Graczyk D, Cieśla M, Boguta M (2018) Regulation of tRNA synthesis by the general transcription factors of RNA polymerase III–TFIIIB and TFIIIC, and by the MAF1 protein. *Biochim Biophys Acta Gene Regul Mech* 1861:320–329.
5. Upadhya R, Lee J, Willis IM (2002) Maf1 is an essential mediator of diverse signals that repress RNA polymerase III transcription. *Mol Cell* 10:1489–1494.
6. Powers RW, 3rd, Kaeberlein M, Caldwell SD, Kennedy BK, Fields S (2006) Extension of chronological life span in yeast by decreased TOR pathway signaling. *Genes Dev* 20: 174–184.
7. Cai Y, Wei Y-H (2016) Stress resistance and lifespan are increased in C. elegans but decreased in S. cerevisiae by mafr-1/maf1 deletion. *Oncotarget* 7:10812–10826.
8. Enyenihi AH, Saunders WS (2003) Large-scale functional genomic analysis of sporulation and meiosis in Saccharomyces cerevisiae. *Genetics* 163:47–54.
9. Bonhoure N, et al. (2015) Loss of the RNA polymerase III repressor MAF1 confers obesity resistance. *Genes Dev* 29:934–947.
10. Willis IM (2018) Maf1 phenotypes and cell physiology. *Biochim Biophys Acta Gene Regul Mech* 1861:330–337.
11. Orioli A, Praz V, Lhôte P, Hernandez N (2016) Human MAF1 targets and represses active RNA polymerase III genes by preventing recruitment rather than inducing long-term transcriptional arrest. *Genome Res* 26:624–635.
12. Mange F, et al.; CycliX Consortium (2017) Diurnal regulation of RNA polymerase III transcription is under the control of both the feeding-fasting response and the circadian clock. *Genome Res* 27:973–984.
13. Schooneman MG, Vaz FM, Houten SM, Soeters MR (2013) Acylcarnitines: Reflecting or inflicting insulin resistance? *Diabetes* 62:1–8.
14. Patel MS, Nemeria NS, Furey W, Jordan F (2014) The pyruvate dehydrogenase complexes: Structure-based function and regulation. *J Biol Chem* 289:16615–16623.
15. Meissen JK, et al. (2016) Phenotyping hepatocellular metabolism using uniformly labeled carbon-13 molecular probes and LC-HRMS stable isotope tracing. *Anal Biochem* 508:129–137.
16. Shambaugh GE, 3rd (1977) Urea biosynthesis I. The urea cycle and relationships to the citric acid cycle. *Am J Clin Nutr* 30:2083–2087.
17. Morris SM, Jr (2002) Regulation of enzymes of the urea cycle and arginine metabolism. *Annu Rev Nutr* 22:87–105.
18. van Waarde A (1988) Operation of the purine nucleotide cycle in animal tissues. *Biol Rev Camb Philos Soc* 63:259–298.
19. Arinze IJ (2005) Facilitating understanding of the purine nucleotide cycle and the one-carbon pool: Part I: The purine nucleotide cycle. *Biochem Mol Biol Educ* 33:165–168.
20. Aragón JJ, Tornheim K, Goodman MN, Lowenstein JM (1981) Replenishment of citric acid cycle intermediates by the purine nucleotide cycle in rat skeletal muscle. *Curr Top Cell Regul* 18:131–149.
21. Lane AN, Fan TW-M (2015) Regulation of mammalian nucleotide metabolism and biosynthesis. *Nucleic Acids Res* 43:2466–2485.
22. Hove-Jensen B, et al. (2016) Phosphoribosyl diphosphate (PRPP): Biosynthesis, enzymology, utilization, and metabolic significance. *Microbiol Mol Biol Rev* 81:e00040-16.
23. Corbin KD, Zeisel SH (2012) Choline metabolism provides novel insights into non-alcoholic fatty liver disease and its progression. *Curr Opin Gastroenterol* 28:159–165.
24. Hermansson M, Hokynar K, Somerharju P (2011) Mechanisms of glycerophospholipid homeostasis in mammalian cells. *Prog Lipid Res* 50:240–257.
25. Wyss M, Kaddurah-Daouk R (2000) Creatine and creatinine metabolism. *Physiol Rev* 80:1107–1213.
26. Kazak L, et al. (2015) A creatine-driven substrate cycle enhances energy expenditure and thermogenesis in beige fat. *Cell* 163:643–655.
27. Kazak L, et al. (2017) Genetic depletion of adipocyte creatine metabolism inhibits diet-induced thermogenesis and drives obesity. *Cell Metab* 26:660–671.
28. Owen OE, Kalhan SC, Hanson RW (2002) The key role of anaplerosis and cataplerosis for citric acid cycle function. *J Biol Chem* 277:30409–30412.
29. Zamboni N, Sauer U (2009) Novel biological insights through metabolomics and 13C-flux analysis. *Curr Opin Microbiol* 12:553–558.
30. Reaves ML, Rabinowitz JD (2011) Metabolomics in systems microbiology. *Curr Opin Biotechnol* 22:17–25.
31. Hackett SR, et al. (2016) Systems-level analysis of mechanisms regulating yeast metabolic flux. *Science* 354:aaf2786.
32. Siskos AP, et al. (2017) Interlaboratory reproducibility of a targeted metabolomics platform for analysis of human serum and plasma. *Anal Chem* 89:656–665.
33. Römisch-Margl W, et al. (2012) Procedure for tissue sample preparation and metabolite extraction for high-throughput targeted metabolomics. *Metabolomics* 8:133–142.
34. Soga T, et al. (2006) Differential metabolomics reveals ophthalmic acid as an oxidative stress biomarker indicating hepatic glutathione consumption. *J Biol Chem* 281:16768–16776.
35. Soga T (2007) Capillary electrophoresis-mass spectrometry for metabolomics. *Methods Mol Biol* 358:129–137.
36. Chong J, et al. (2018) MetaboAnalyst 4.0: Towards more transparent and integrative metabolomics analysis. *Nucleic Acids Res* 46:W486–W494.
37. Goldman A, Harper S, Speicher DW (2016) Detection of proteins on blot membranes. *Curr Protoc Protein Sci* 86:10.8.1–10.8.11.
38. Fay DS, Gerow K (2013) A biologist's guide to statistical thinking and analysis. *WormBook,* 1–54.